IEEE Access
Multidisciplinary ⋮ Rapid Review ⋮ Open Access Journal

Received 5 July 2024, accepted 12 August 2024, date of publication 20 August 2024, date of current version 30 August 2024.

Digital Object Identifier 10.1109/ACCESS.2024.3446626

RESEARCH ARTICLE

Construction of a Deterministic Binary Chaotic Compressed Sensing Measurement Matrix Utilizing Householder Orthogonalization and Pseudorandom Number Transformation

XUANWEI ZHANG AND HUIMIN YU
College of Information Science and Engineering, Hunan Normal University, Changsha 410081, China
Corresponding author: Huimin Yu (yhm@hunnu.edu.cn)

ABSTRACT The development of measurement matrices remains a pivotal focus within the domain of compressed sensing theory. This paper introduces an innovative methodology for the construction of a deterministic binary measurement matrix, harnessing the properties of chaotic sequences. This approach streamlines the process and only requires a fixed number of initial variables for matrix construction. The construction method of the measurement matrix is divided into two distinct stages. Initially, the matrix elements are extracted through gapless sampling of chaotic sequences. Recognizing the inherent correlation among chaotic sequence elements due to gapless sampling, this paper introduces a novel nonlinear binary transformation. This innovative approach effectively mitigates the correlation and concurrently addresses storage limitations. Thereafter, the entries are integrated into a Toeplitz matrix, leveraging its structured row and columnar properties to augment storage efficiency. In subsequent steps, the approach integrates the Householder transformation to generate an orthogonal basis, thereby enhancing the matrix's performance. Additionally, an XOR operation is employed to optimize the distribution of entries across each column vector. The research substantiates that the resultant matrix exhibits low correlation, is facile in generation, and amenable to reconstruction. Comprehensive experimental data corroborate the efficacy of the constructed measurement matrix in processing both one-dimensional and two-dimensional signals. The matrix demonstrates a strong potential to meet the Restricted Isometry Property (RIP), thereby underscoring its substantial advantages across a myriad of considerations.

INDEX TERMS Compressed sensing, deterministic measurement matrix, chaotic sequences, restricted isometry property.

I. INTRODUCTION

Compressed Sensing (CS), pioneered by Donoho et al. [1], represents an innovative paradigm in signal sampling. The CS framework encompasses sampling, compression, and signal reconstruction phases. Pivotal areas of research within this domain are the selection of sparse matrices, the crafting of measurement matrices, and the refinement of signal reconstruction algorithms. CS is predicated on the principle that signals which are sparse in their original form or within a transformed domain can be accurately recovered from a subset of measurements. The construction of the measurement matrix stands as a cornerstone of CS theory, exerting a profound impact on the fidelity of both signal acquisition and reconstruction. The broad applicability of CS is becoming increasingly apparent, with its utility extending to a spectrum of disciplines and practical applications. In the context of vibration signal acquisition, sensor failures and transmission issues can cause data loss, which is treated as a stochastic CS scenario. Utilizing CS reconstruction algorithms enables the recovery of the original signal from incomplete data, addressing data recovery.

The associate editor coordinating the review of this manuscript and approving it for publication was Fang Yang.

Moreover, CS techniques aid in the swift identification of sensor malfunctions and curtail network communication loads by extracting system status from a constrained set of sensor readings. Notable other examples include the processing of electrocardiogram (ECG) signals [2], the reconstruction of video data via compressive sensing techniques [3], and SAR image reconstruction via CS incremental imaging [4].

To evaluate the suitability of measurement matrices, Candes and Tao introduced the seminal Restricted Isometry Property (RIP) [5], a criterion that certifies a matrix's ability to faithfully reconstruct original signals from their low-dimensional projections. Measurement matrices are traditionally classified into two categories: random and deterministic. Initially, CS research predominantly utilized random matrices, such as Gaussian [6] and Bernoulli [7] matrices, which, despite fulfilling the RIP conditions, present significant challenges due to their inherent lack of structure. This results in high demands for storage and computational resources. In response, deterministic matrices have risen in prominence, providing structured alternatives including the Fourier matrix [8]; matrices derived from optimal codebooks and codes [9]; and low-coherence explicit matrix based on algebraic geometry coding [10].

Chaotic sequences, endowed with inherent randomness and nonlinearity, have risen as auspicious contenders for the construction of compressed sensing measurement matrices [11]. Recognizing their desirable attributes, researchers have advocated for their utilization in the formulation of such matrices, exemplified by the development of a dynamic sparse circulant measurement matrix leveraging a novel compound Sine chaotic map [12]; matrices predicated on Chebyshev chaotic sequences [13]; and matrices generated through a 2D-SLIM mapping technique [14]. Additionally, an orthogonal matrix, underpinned by a nonlinear chaotic system, has been introduced for compressive sensing applications [15]. However, traditional approaches to constructing measurement matrices from chaotic sequences necessitate meticulous attention to sampling intervals to mitigate cross-correlation among data points, a requirement that can engender data redundancy. To ameliorate the efficiency of signal processing, the present study introduces an enhanced methodology that integrates a variety of chaotic sequences, culminating in the advancement of a superior measurement matrix.

The primary contributions of this paper are as follows:

1. The paper introduces an innovative methodology for constructing deterministic binary measurement matrices, employing a variety of chaotic maps. Rigorous validation has established that this novel approach not only adheres to the RIP but also excels in performance compared to conventional measurement matrices.

2. The paper presents a novel nonlinear binary transformation and a method for the selection of high-quality orthogonal bases via Householder transformation, both of which serve to augment matrix performance.

3. This study achieves a substantial reduction in the length of initial variables and the storage space requisite for the generation of the measurement matrix. This reduction in resource demands facilitates cost savings and enhances the efficiency of resource utilization.

II. CAMPRESSED SENSING THEORY

Compressed sensing theory represents a breakthrough from the constraints of the Nyquist-Shannon sampling theorem, alleviating data sampling, storage, transmission, and analysis burdens significantly. If a one-dimensional signal $x \in R^N$ contains k non-zero elements (where $k \ll N$), it is considered sparse. While most time domain signals lack inherent sparsity, they can be represented sparsely under an orthogonal basis set as expressed by the equation:

$$x = \Psi\alpha \tag{1}$$

Here, $\Psi \in R^{N\times N}$ represents a sparse matrix, $\alpha \in R^N$ denotes a sparse coefficient, and the sparse coefficient exhibits sparsity. For a sparse signal $x \in R^N$, compression and sampling are achieved using a measurement matrix $\Phi \in R^{M\times N}(M \ll N)$ to derive the observation value $y \in R^M$, formulated as:

$$y = \Phi\Psi\alpha \tag{2}$$

The RIP enforces a Restricted Isometry Constant (RIC) $\delta_k \in (0, 1)$, ensuring:

$$(1-\delta_k)\| x \|_2^2 \le \| \Phi x \|_2^2 \le (1+\delta_k)\| x \|_2^2 \tag{3}$$

Under this property, the ℓ_0 norm can be utilized to compute α [16]. As the ℓ_0 norm optimization is non-deterministic polynomial (NP) problem, the ℓ_1 norm serves as a convex approximation [17], yielding the following formulation:

$$min\| \alpha \|_{\ell_1}, \qquad s.t.y = \Phi\Psi\alpha. \tag{4}$$

Verifying the RIP property directly may be challenging in practical scenarios, prompting the examination of alternative characteristics. Baraniuk and collaborators established that RIP equivalence corresponds to the requirement that the measurement matrix Φ be uncorrelated with the sparse matrix Ψ. Matrix incoherence measures the extent of correlation between any rows and columns of two matrices in incoherent measurements, ensuring that rows of Φ cannot depict columns of Ψ sparsely. The mutual coherence [18] is defined as:

$$\mu(\Phi, \Psi) = \sqrt{N} max \left|\phi_k, \psi_j\right| \tag{5}$$

Here, $k \in [1, M]$ and $j \in [1, N]$. A lower μ value indicates decreased correlation between Φ and Ψ, implying greater direction distinction post-transformation—resulting in diminished measurement requirements for accurate restoration from low-dimensional samples of the initial information.

III. MEASUREMENT MATRIX CONSTRUCTION

A. NONLINEAR BINARY TRANSFORMATION

Chaotic sequences are distinguished by a suite of attributes, including superior pseudo-random characteristics, the unpredictability of their orbital patterns, and a pronounced sensitivity to initial conditions and regulatory parameters [19]. In this paper, we propose a synthesis of orthonormal matrices with chaotic sequences, aimed at fabricating a deterministic measurement matrix that boasts heightened performance. The deterministic nature of the Toeplitz matrix is underscored by its structured statistical correlations across both its rows and columns—a feature derived from the convolution inherent in linear system identification [20]. This matrix's generation, predicated on a set of predefined instances, optimizes storage efficiency. Furthermore, the orthonormal matrix plays a pivotal role in dispersing the informational content of signal samples across all measurement points within the compression and measurement phase [21].

For a map, the generation of a sequence is governed by the following equation:

$$f\left(z_i\right) = f^i\left(z_0\right), i \in Z^+ \tag{6}$$

Here, z_0 represents the initial condition of the chaotic map, i represents the number of iterations and the selection of appropriate system parameters is also essential. Once the initial value and parameters are specified, the iterative process of the chaotic map yields a sequence of the desired length. This sequence, while deterministic in nature, is entirely dictated by the mapping function, the system parameters, and the initial conditions of the underlying nonlinear dynamical system. The reproducibility of the entire sequence, given identical system parameters and initial conditions, forms the foundational principle for the construction of a deterministic measurement matrix.

Given that the total length of the generated chaotic sequence is denoted by $2N_0$, where N_0 represents a specific positive integer, the sequence is partitioned into two distinct segments. These segments are designated for subsequent processing:

$$\begin{cases} Z_1' = \left\{f^i\left(z_0\right)\right\}_{i=1}^{N_0} \\ Z_2' = \left\{f^i\left(z_0\right)\right\}_{i=N_0+1}^{2N_0} \end{cases} \tag{7}$$

Let the sequence Z' be an element of the interval (a, b). We apply the subsequent transformation to the elements of Z:

$$Z = \frac{2\left(Z' - a\right)}{b - a} - 1 \tag{8}$$

At this juncture, the elements of the sequence Z are symmetrically distributed about an interval centered at zero.

Lemma 1 ([22]): Suppose there exist independent random variables Z_1 and Z_2.

$$\begin{cases} U_1 = \sqrt{-2\ln(Z_1)} \times \cos\left(2\pi Z_2\right) \\ U_2 = \sqrt{-2\ln(Z_1)} \times sin\left(2\pi Z_2\right) \end{cases} \tag{9}$$

The resulting U_1 and U_2 are also independent random variables.

According to the above formula, the following relationship can be obtained:

$$\begin{cases} Z_1 = \exp\left(\dfrac{-\left(U_1^2 + U_2^2\right)}{2}\right) \\ Z_2 = -\dfrac{1}{2\pi} arctan \dfrac{U_2}{U_1} \end{cases} \tag{10}$$

The joint probability density of U_1 and U_2 can be obtained as:

$$\begin{aligned} f\left(U_1, U_2\right) &= \frac{1}{2\pi} exp\left(\frac{-\left(U_1 + U_2\right)}{2}\right) \\ &= \frac{1}{2\pi} exp\left(\frac{-U_1^2}{2}\right) \cdot exp\left(\frac{-U_2^2}{2}\right) \\ &= f(U_1) f(U_2) \end{aligned} \tag{11}$$

It can be observed from the above formula that the probability density of $f\left(U_1, U_2\right)$ is constant on a circle with a square radius of $U_1^2 + U_2^2$, which means that the range of $arctan\, U_2/U_1$ is evenly distributed in the interval $(0, 2\pi)$. $-2\ln\left(Z_1\right)$ or $-2\ln\left(Z_2\right)$ follows a Chi-square distribution with two degrees of freedom. This approach can be viewed as a method for generating random variables from a pseudo-random sequence. The sequences U_1 and U_2 are transformed into binary sequences W_1 and W_2, respectively, by employing the sign function. In a random sequence, each datum is independent, exhibiting stochastic variability, and is unaffected by other data points. Consequently, the correlation between data points is inherently random, both in the original and the binary sequences obtained post-conversion. The application of the sign function for conversion preserves the mutual independence and the stochastic nature of the data points. Thus, for random sequences, the transformation to a binary format via the sign function does not alter the inherent randomness and decorrelation among the sequences.

A chaotic sequence generated by a single map may encounter limitations, such as an uneven distribution when the parameter range is narrow during the full mapping of the Logistic map, or a tendency to enter a periodic loop state after a certain number of iterations of the Chebyshev sequence due to finite accuracy constraints. Additionally, limited computational resources may hinder the sequence from achieving desirable pseudo-random qualities. Recognizing that the measurement matrix's performance is contingent upon the properties of the chaotic sequence. Therefore, this paper introduces a hybrid chaotic mapping array to optimize the distribution of entries in the column vector of the measurement matrix.

B. MATRIX CONSTRUCTION STEPS

The procedure for constructing a deterministic matrix based on chaotic sequences (assuming the matrix dimension is $M \times N$.) comprises the following steps:

Step (1): Employ equation (6) to generate a chaotic sequence with a length of $2N$. Subsequently, partition this sequence into two equal subsequences, X_1 and X_2, each of length N. Employ equation (8) to transform the sequences X_1 and X_2 into $X_1'=\{x_\tau\}_{i=1}^{N}$ and $X_2'=\{x_\tau\}_{i=N+1}^{2N}$, respectively, such that they exhibit a symmetric distribution about the origin.

Step (2): Utilize the formula below to convert them into binary sequences W_1 and W_2, which are relatively independent:

$$\begin{cases} W_1 = sign\left(\sqrt{-2\ln(X_1')} \times \cos\left(2\pi X_2'\right)\right) \\ W_2 = sign\left(\sqrt{-2\ln(X_1')} \times sin\left(2\pi X_2'\right)\right) \end{cases} \tag{12}$$

The procedure retains the real component of W_1 and W_2, and subsequently transforms it into a binary sequence.

Step (3): Enter the entries of $W_1=\{u_\tau\}_1^N$ and $W_2=\{r_\tau\}_1^N$ into the Toeplitz matrix. Construct the $N\times N$ Toeplitz matrix T as follows:

$$\mathrm{T}=\begin{bmatrix} u_1 & r_2 & \cdots & r_N \\ u_2 & u_1 & & r_{N-1} \\ \vdots & & \ddots & \vdots \\ u_{N-1} & u_{N-2} & \cdots & r_2 \\ u_N & u_{N-1} & & u_1 \end{bmatrix} \tag{13}$$

Algorithm 1 Measurement Matrix Construction Algorithm

Input: Chaotic map $f\left(z_i\right)=f^i\left(z_0\right), z_i\in(a,b)$.
Output: Measurement matrix Φ
For $j=1,2,3,\cdots,2N$
$X_1'=\left\{\frac{2(f^j(x_0)-a)}{b-a}-1\right\}_{j=1}^{N}$
$X_2'=\left\{\frac{2(f^j(x_0)-a)}{b-a}-1\right\}_{j=N+1}^{2N}$
End
$W_1=sign\left(\sqrt{-2\ln\left(X_1'\right)}\times\cos\left(2\pi X_2'\right)\right)=\{u_\tau\}_1^N$
$W_2=sign\left(\sqrt{-2\ln\left(X_1'\right)}\times\sin\left(2\pi X_2'\right)\right)=\{r_\tau\}_1^N$
For $i=1,2,3,\cdots,N$
$NV=W_1\oplus W_2=\{nv_i\}_{i=1}^N$
$t_i=\left[r_i,r_{i-1},\cdots r_2,u_1,u_2,\cdots,r_{N-i+1}\right]^T$
$\mathrm{T}=[t_1,t_2,\cdots t_N]$
End
For $k=1,2,3,\cdots,N-1$
Set $x=t_k\left(i\right), i=k,k+1,\cdots,N, e_1=[1,0,\cdots 0]^T$
$\vartheta_k=t_k+sign\left(t_k\left(1\right)\right)\|t_k\|e_1$
$Z_k=\left[t_k\left(i\right),t_{k+1}\left(i\right),\cdots t_N\left(i\right)\right]$
$Z_k=Z_k-2\vartheta_k\left(\vartheta_k^T Z_k\right)$
$V_k=\left[v_k,v_{k+1},\cdots v_N\right]$
$V_k=V_k-2\left(V_k\vartheta_k\right)\vartheta_k^T$
$\mathrm{V}=[v_1,v_2,\cdots v_N]$
End
For $i=1,2,\cdots,N$
If $nv_i==-1$
$v_i=-v_i$
End
End

Obtain a set of orthogonal basis vectors for the matrix T through Householder transformation, and transform it into binary using the symbol function, get matrix $\mathrm{V}\in R^{N\times N}$. Select the first M rows of the standardized matrix $\mathrm{V}=[v_1,v_2,\cdots v_N]$ as the optimized orthogonal basis.

Step (4): Apply the XOR operation to the random sequences W_1 and W_2 to derive a column vector of flip coefficients that are uniformly distributed and exhibit stochastic independence.

$$NV=\{nv_\tau\}_{\tau=1}^N=W_1\oplus W_2 \tag{14}$$

Among them $nv_\tau\in\{-1,1\}$. When $nv_\tau=-1$, select the τ-th column vector v_τ from the orthogonal basis V to perform a negation operation.

Follow the steps above, the construction method of the measurement matrix is summarized as Algorithm 1:

IV. RIP CONDITION ANALYSIS

For the sequence $X_1'=\{x_\tau\}_{i=1}^N$ and $X_2'=\{x_\tau\}_{i=N+1}^{2N}$, the chaotic sequence is generated through an iterative process. Consequently, the following relationship holds:

$$X_2'=\left\{f^N\left(X_1'\right)\right\} \tag{15}$$

Consequently, within the scope of this methodology, the value indicated by equation (9) is determined by the initial condition x_0 of the chaotic sequence:

$$U\begin{cases} \left\{\sqrt{-2\ln\left(f^i\left(x_0\right)\right)}\times\cos\left(2\pi f^N\left[f^i\left(x_0\right)\right]\right)\right\}_{i=1}^N \\ \left\{\sqrt{-2\ln\left(f^i\left(x_0\right)\right)}\times\sin\left(2\pi f^N\left[f^i\left(x_0\right)\right]\right)\right\}_{i=1}^N \end{cases} \tag{16}$$

The binary conversion method can be encapsulated within the following process, which employs a specific transformation function, denoted as $T(\cdot)$:

$$T\left(f^i\left(x_0\right)\right)=\begin{cases} 1 & for\ U>0 \\ -1 & for\ U<0 \end{cases} \tag{17}$$

This function orchestrates the conversion of input data into a binary format. Given the sequences X_1' and X_2', which are generated under identical initial conditions and system parameters, they exhibit the same probability density function. This property is expressed as follows: $\rho\left(X_1'\right)=\rho\left(X_2'\right)$. Consequently, W_1 and W_2 are characterized by an identical probability distribution. The chaotic sequence exhibits a binary distribution, where $T\left(x_l\right)=T\left[f^i\left(x_0\right)\right]_{i=1}^l$, a state set S exists, which is defined as follows:

$$S=\{g_1=T\left(x_1\right),g_2=T\left(x_2\right),\cdots g_l=T\left(x_l\right)\} \tag{18}$$

where $\{g_1,g_2,\cdots g_l\}\in\{-1,1\}$.

Lemma 2 ([23]): If a Perron-Frobenius operator P acts on a function $F(x)$ with bounded variation of $G(x)$, then the resulting operation satisfies:

$$P\{F(x)\}=\frac{d}{dx}\int F(y)dy=\sum\left|\left(G^{-1}\left(y\right)\right)'\right|F(y) \tag{19}$$

When $F(x) = T(x) \cdot \rho(x)$, there exists:

$$P\{T(x)\,\rho(x)\} = E_T\,\rho(x) \tag{20}$$

Among them:

$$E_T = \sum T(x_l) \cdot Pro\{S\} \tag{21}$$

Theorem 1: For binary sequences $T(x_l)$ of different lengths, there exists: $E\left[T\left(x_{l_1}\right)T\left(x_{l_2}\right)\right] = E\left[T\left(x_{l_1}\right)\right] E\left[T\left(x_{l_1}\right)\right]$.

Proof: According to the Perron-Frobenius operator in Lemma 1, we can obtain:

$$\begin{aligned} &E\left[T\left(x_{l_1}\right)T\left(x_{l_2}\right)\right] \\ &= \int P\left\{T\left(x_{l_1}\right)\rho(x)\right\} \cdot \left\{T\left(x_{l_2}\right)\right\} dx \\ &= E\left[T\left(x_{l_1}\right)\right] \int \rho(x)\left\{T\left(x_{l_2}\right)\right\} dx \\ &= E\left[T\left(x_{l_1}\right)\right] E\left[T\left(x_{l_2}\right)\right] \end{aligned} \tag{22}$$

The Quantile-Quantile (Q-Q) plot is a statistical chart method used to assess if data adheres to a particular distribution. In the Q-Q plot, the quantiles of one data set are juxtaposed with the theoretical quantiles of another data set with the identical distribution [24], typically shown as a straight line or curve. When the data aligns well with the designated distribution, the points will roughly fall on the diagonal line. Here we test whether the entries of the U_1 and U_2 satisfy the normal distribution and obtain the Q-Q plot as shown in Fig. 1. Analysis of the figure reveals that the sequences U_1 and U_2 are approximately Gaussian distributed. Consequently, the elements within the sequences W_1 and W_2 exhibit characteristics that are consistent with this distributional assumption.

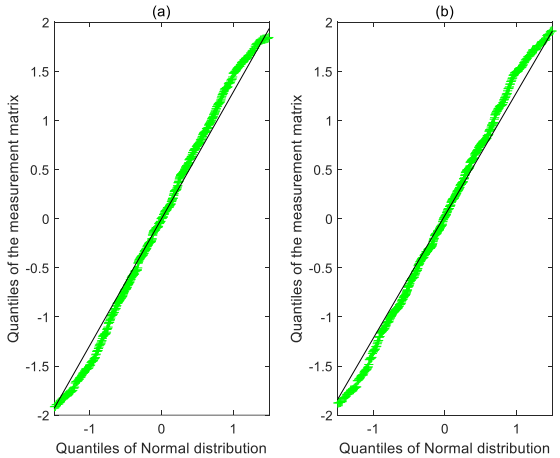

FIGURE 1. Q-Q plots comparing the distribution of entries of U_1, U_2 and Gaussian distribution. (a) Q-Q plot for U_1. (b) Q-Q plot for U_2.

Upon analysis, it is evident that the elements within the sequences W_1 and W_2 adhere to the property of independent and identical distribution, characterized by their stochastic independence. Since each column of the constructed Toeplitz matrix T is linearly independent, this implies that the rank of matrix T is $rank(T) = N$. Consequently, the matrix T is proven to be invertible, a property that is fundamental in the context of linear algebra. The Householder transformation [25], a prevalent method for matrix manipulation, serves to convert a matrix into its orthogonal counterpart. This transformation is widely applied across various domains, including QR decomposition, the computation of eigenvalues, and the orthogonalization of matrices. Since matrix T is a real-valued matrix, each column vector of this matrix is an eigenvector of T′T. For a $N \times N$ matrix T, let G = T′T, where the diagonal elements are given by $G_{ii} = \sum_{j=1}^{M} t_j^2$, with $0 \le t_j^2 \le c, c \ge 1$. According to the properties of the Toeplitz matrix [20], if matrix T satisfies the K-order isometry constraint and $\delta_K \in (0,1)$, when $K \ge 1$, if there exist positive numbers δ_1 and δ_2 such that $\delta_1 + \delta_2 = \delta_K$, then each diagonal element in matrix G satisfies $|G_{ii} - 1| < \delta_1$, and the non-diagonal elements satisfy $G_{ij} < \left(\delta_2/K\right)$. The RIP describes the conditions under which a nonlinear measurement sequence possesses a feasible sparse solution. The lower the correlation, the better the reconstruction effect. In this context, Householder transformation is utilized to obtain an orthogonal matrix with low correlation.

In this context, it is imperative to verify that the elements within the rows or columns of the orthogonal matrix are not entirely equivalent, thereby employing the process of random column inversion to preclude the matrix from degrading to a certain value. Consequently, a symbol sequence NV, characterized by its superior randomness, is generated. This sequence is derived from the XOR operation applied to W_1 and W_2. The operation imparts an enhanced random distribution to the resultant binary sequence without altering the distribution state of its elements. The NIST's standard method for pseudo-random number testing is utilized for verification [26], subjecting the symbol sequence NV to fifteen distinct tests. With a test sequence length of $1e7$, exceeding the minimum length recommended for NIST testing, a test is considered passed if the P_{value} exceeds 0.01. The test is conducted one hundred times to ascertain the pass rate, denoted as P_{rate}. The outcomes are presented in Table 1. Examination of the table reveals that the column flip sign vector possesses desirable random properties, with the probabilities $P(nv_\tau = 1)$ and $P(nv_\tau = -1)$ each equating to $1/2$. Consequently, this ensures that the robustness of the matrix is maximized.

Theorem 2 ([27]): Let $q \in R^m$ be a vector with a finite p-norm, i.e., $\|q\|_p < \infty$. When the chaotic orthogonal binary matrix, referred to as VCM and developed in this paper, is utilized, there exists: $k_1 \|q\|_p^2 \le \left|\sum_{j=1}^{m} \langle q, \theta_j \rangle\right|^2 \le k_2 \|q\|_p^2$, $0 < k_1 \le k_2 < \infty$.

Proof: If $\Theta^T\Theta = \mathrm{V}\Sigma\mathrm{V}^T$, The j-th eigenvalue of Σ is expressed as: $\Sigma_{jj} = \vartheta_j$, it gives:

$$\left|\sum_{j=1}^{m} \langle q, \theta_j \rangle\right|^2 = \langle q, \mathrm{V}\Sigma\mathrm{V}^T q \rangle = \langle \mathrm{V}^T q, \sum \mathrm{V}^T q \rangle \tag{23}$$

TABLE 1. NIST testing results.

Statistical tests	P_{value}	P_{rate}
FT	0.798139	0.99
BFT	0.955835	1.00
CST	0.474986	0.99
RT	0.897763	0.99
LROT	0.964295	1.00
MRT	0.013569	0.99
SPT	0.739918	1.00
NTMT	0.935716	0.99
OTMT	0.162606	0.98
MUST	0.739918	1.00
AET	0.191687	1.00
RET	0.492448	0.98
REVT	0.806258	0.97
ST	0.437274	0.99
LCT	0.020548	0.97

Since V is an orthogonal matrix, there exists: $q^T \mathrm{V}\mathrm{V}^T q = q^T q$, $\alpha = V^T q$, therefore:

$$\left|\sum_{j=1}^{m} \langle q, \theta_j \rangle\right|^2 = \langle \mathrm{V}^T q, \Sigma \mathrm{V}^T q \rangle = \sum_{j=1}^{m} \vartheta_j \left|\alpha_j\right|^2 \tag{24}$$

We can obtain:

$$\vartheta_{min} \left\|q\right\|_2^2 \leq \sum_{j=1}^{m} \vartheta_j \left|\alpha_j\right|^2 \leq \vartheta_{max} \left\|q\right\|_2^2 \tag{25}$$

Let $\mathrm{S} = \mathrm{V}\Psi = \left\{s_1, s_2, \cdots s_N\right\}$, $\Psi = \left\{\psi_1, \psi_2, \cdots \psi_N\right\}$ be a sparse matrix with orthogonal column vectors. The order of magnitude of Ψ is approximately $O(logN/N)$, close to $O(1/\sqrt{N})$. In this context, we can express:

$$s_{ij} = \langle h_i \psi_j \rangle = \sum_{k=1}^{N} v_{ik} \psi_{kj} \tag{26}$$

Hence, the expectation of s_{ij} is:

$$E\left(s_{ij}\right) = E\left(\sum_{k=1}^{N} v_{ik} \psi_{kj}\right) = 0 \tag{27}$$

Then the variance of s_{ij} is:

$$\begin{aligned} \sigma^2 &= E\left(s_{ij}^2\right) - E^2(s_{ij}) = E(s_{ij}^2) \\ &= E\left(\sum_{k=1}^{N} v_{ik}^2 + \sum_{k=1}^{N}\sum_{k'=1}^{N} v_{ik} v_{ik'}\right) \sum_{k=1}^{N} \psi_{kj}^2 \\ &= E\left(\sum_{k=1}^{N} v_{ik}^2\right) \sum_{k=1}^{N} \psi_{kj}^2 \end{aligned} \tag{28}$$

Lemma 3 ([28]): The Central Limit Theorem(CLT): If there are independent and identically distributed random variables $z_1, z_2, \cdots, z_N$, there is an expectation $E\left(z_k\right) = 0 (k = 1, 2, 3, \cdots, N)$, and the variance is σ_z^2, then for The sum of random variables $z = \sum_{k=1}^{N} z_k$, $\sigma^2 = \sum_{k=1}^{N} Var(z_k)$. If a given constant $\varepsilon > 0$ and N is large enough, z approximately obeys $(0, N\sigma_z)$, and the following inequality exists: $\sigma_z^2 < \varepsilon\sigma^2$.

In describing the N-order orthogonal matrices V and Ψ, the order of magnitude of the maximum absolute value of all elements in the matrix is $O(1/\sqrt{N})$. For $v_{ik}\psi_{kj}$, there exist positive constants c_1 and c_2 ($c_1 < c_2$), such that:

$$\frac{c_1}{N}\psi_{kj}^2 \leq Var(v_{ik}^2 \psi_{kj}^2) \leq \frac{c_2}{N}\psi_{kj}^2 \tag{29}$$

Hence, for s_{ij}:

$$\frac{c_1}{N} = \frac{c_1}{N}\sum_{k=1}^{N}\psi_{kj}^2 \leq \sigma^2 \leq \frac{c_2}{N}\sum_{k=1}^{N}\psi_{kj}^2 = \frac{c_2}{N} \tag{30}$$

According to the CLT: for independent random variables and s_{ij} with $E(s_{ij}) = 0$, it converges to a normal distribution $N(0, \sigma^2)$ and follows a Gaussian asymptotic distribution. NV is a random sequence satisfying Bernoulli distribution, preventing $\mathrm{V}\Psi$ from degenerating into a specific value. For the measurement matrix $\Phi = \mathrm{V}$, if the maximum absolute value of all elements in the sparse matrix Ψ is of the order of magnitude $O(1/\sqrt{N})$, the mutual interference $\mu = max_{1\leq i,j\leq N}\left|s_{ij}\right|$ is derived by randomly selecting the highest value of the sequence and the union:

$$\Pr\left(max_{1\leq i,j\leq N}\left|s_{ij}\right| \leq t_1\right) \geq 1 - 2N^2 \exp\left(\frac{-t_1^2}{2\sigma^2}\right) \tag{31}$$

where $\delta \in (0, 1)$, when $t_1 = \sqrt{2\sigma^2 \log\left(N^2/\delta\right)}$, the above formula can be transformed into:

$$\Pr\left(max_{1\leq i,j\leq N}\left|s_{ij}\right| \leq \sqrt{2\sigma^2 \log\left(\frac{2N^2}{\delta}\right)}\right) \geq 1 - \delta \tag{32}$$

where the variance is $\sigma^2 = \sum_{k=1}^{N} Var\left(v_{ik}^2\psi_{kj}^2\right)$, and there exists a constant c_0 such that:

$$\sigma^2 \leq \frac{c_0}{N}\sum_{k=1}^{N}\psi_{kj}^2 = \frac{c_0}{N} \tag{33}$$

where $0 \leq c_0 \leq N$, $c_0 \in Z^+$, $t_0 = \left[2\left(c_0/N\right)\log\left(N^2/\delta\right)\right]^{1/2}$, the upper bound of the coherence of the matrices Φ and Ψ is $O\left(\left(\log\left(N/\delta\right)/N\right)^{1/2}\right)$, which is closest to the optimal value except for the $logN$ factor.

Theorem 3: If there are constants c_3, c_4, if $M \geq \left(c_3 \cdot n \cdot log\left(N/n\right)\right)$, where $n < N$, the probability that VCM satisfies RIP is $1 - 2exp(-c_4 M)$.

Proof: For each n-dimensional space, there are the following probabilities [29]:

$$P \leq 2\left(\frac{12}{\sigma}\right)^n \cdot exp\left(-c\left(\frac{\sigma}{2}\right)M\right) \tag{34}$$

where $0 < \sigma < 1$, Since VCM has $\binom{N}{n}$ sub-matrices, the probability that VCM satisfies RIP should be:

$$\begin{aligned} P &\leq 2\binom{N}{n} \cdot \left(\frac{12}{\sigma}\right)^n \cdot exp\left(-c\left(\frac{\sigma}{2}\right)M\right) \\ &\leq 2exp\left[-c\left(\frac{\sigma}{2}\right)M + n\left(log\frac{eN}{n} + log\frac{12}{\sigma}\right)\right] \end{aligned} \tag{35}$$

V. PERFORMANCE ANALYSIS

To facilitate the measurement of the performance of the constructed measurement matrix, it is compared with other matrices, evaluate matrix performance by calculating metrics such as correlation coefficients and complexity. The selected matrices are shown in Table 2.

TABLE 2. Measurement matrices.

Abbreviation	Full name
GM	Gaussian Matrix
MCBM [30]	Mixed Chaotic Bernoulli Matrix
BM-C [31]	Chaotic Bipolar Measurement Matrix
SBM [32]	Symbolic Bernoulli Matrix
COM [15]	Chaotic Orthogonal Matrix
LTSBM [33]	Logistic-Tent-Sine Bernoulli Matrix
VCM	Proposed in this paper

A. CORRELATION ANALYSIS

1) THE GM

GM can generate random numbers distributed between $(-1, 1)$. $R_{ij} = \left\langle \phi_i, \psi_j^T \right\rangle = \sum_{k=1}^{N} \phi_{ik} \psi_{kj}^T$, since $E(\phi_{ik}) = 0$, so for $z_k = \phi_{ik}\psi_{kj}^T$ exists $E(z_k) = 0$.

Lemma 4 ([34]): The Hoeffding Inequality: If there are independent random variables $z_1, z_2, \cdots, z_N$, if $c_k \le z_k \le e_k (k = 1, 2 \cdots, N)$, then there is $t_1 > 0$ such that:

$$\Pr\left(max_{1\le i,j\le N} \left| \sum_{k=1}^{N} z_k - E\left(\sum_{k=1}^{N} z_k \right) \right| \le t_1 \right) \ge 1 - 2\exp\left(\frac{-2t_1^2}{\sum_{k=1}^{N} (c_k - e_k)^2} \right) \tag{36}$$

Since $-1 < \phi_{ik} < 1$, and $E(z_k) = 0$, then:

$$\Pr\left(max_{1\le i,j\le N} \left| R_{ij} \right| \ge t_1 \right) < 2\exp\left(\frac{-t_1^2}{2N} \right) \tag{37}$$

Therefore:

$$\mu_{GM} > \sqrt{2N \log\left(\frac{2}{\delta} \right)} \tag{38}$$

2) THE COM

The COM exists $M_{ij} = \sum_{k=1}^{N} h_{ik} \psi_{kj}$, Similar to the method in the previous section, the mutual interference of this matrix is:

$$\mu_{COM} = \sqrt{\frac{2\log\left(2N^2/\delta\right)}{N}} \tag{39}$$

3) THE LTSBM, SBM, AND MCBM

For LTSBM and SBM, there exists $-1 \le \phi_{ik} \le 1$, and $E(\phi_{ik}) = 0$. According to Lemma 4, when $t_1 = \left[2N \log\left(2/\delta\right)\right]^{1/2}$, there exists:

$$\Pr\left(max_{1\le i,j\le N} \left| B_{ij} \right| \ge \sqrt{2N \log\left(\frac{2}{\delta} \right)} \right) \le \delta \tag{40}$$

Therefore:

$$\mu_{LTSBM} = \mu_{SBM} = \mu_{MCBM} = \sqrt{2N \log\left(\frac{2}{\delta} \right)} \tag{41}$$

Given that the XOR operation preserves the distribution of sequences, in the context of the MCBM, the resultant matrix entries adhere to a Bernoulli distribution. This is achieved through the XOR operation between the Logistic and Chebyshev symbol sequences, they have similar correlation coefficients.

4) THE BM-C

Lemma 5 ([31]): If there exists a BM-C $Q \in R^{M\times N}$, an arbitrary unit vector $l \in R^N$, for $0 < \gamma < 1$ and a constant $b(\gamma)$ such that:

$$\Pr\left(\|Q \cdot l\|^2 \ge 1 + \gamma \right) \le exp\left(-\left(\frac{\gamma^2}{4} - \frac{\gamma^3}{6} \right) M \right) \tag{42}$$

The BM-C also meets the above conditions of LTSBM and SBM.

According to the above analysis, we can get: $\mu_{GM} > \mu_{LTSBM} = \mu_{SBM} = \mu_{MCBM} \approx \mu_{BM-C} > \mu_{VCM} = \mu_{COM}$. The lower the correlation of the matrix, the greater the possibility of satisfying RIP [35]. Gaussian random measurement matrices satisfy RIP with high probability, and the VCM constructed in this paper have lower correlation than Gaussian random measurement matrix of the same size. Therefore, VCM can better satisfy RIP, and compared with other five measurement matrices, VCM has stronger reconstruction performance. The MCBM, LTSBM, SBM, and BM-C have similar probabilities of satisfying the RIP condition, and the probabilities are all greater than those of the GM, but smaller than those of the VCM and the COM.

B. COMPLEXITY ANALYSIS

If it is necessary to construct an $N \times N$ measurement matrix, the construction method outlined in this paper only requires generating a chaotic sequence with a total length of $2N$. This approach avoids the issue of sequence irrelevance, which is typically encountered when using chaotic sequences that require sampling distance to ensure correlation. Additionally, a structured Toeplitz matrix is utilized to conserve storage resources. This matrix is generated line by line according to a predetermined optimal order. For v_i, where NV is obtained through XOR operation. Following the basic concept of Householder transformation, we can obtain v_i. Using a vector to store the orthonormal matrix based on Householder transformation is a more efficient approach, requiring only $N + Nlog_2N$ bits for storage. Among them, the orthonormal matrix V requires $Nlog_2N$ bits, while the mixed chaotic sequence NV requires N bits. For the GM, storage of nN^2 bits are necessary. Here, n represents the number of non-integer bits. The GM is non-deterministic, requiring more memory space in practical applications. On the other hand, the assembly of the MCBM necessitates the utilization of two

distinct chaotic sequences in the matrix formation process. This requirement implies a heightened demand for initial variable allocation. MCBM, BM-C, SBM, COM and LTSBM all require generating N^2 initial variables for constructing the measurement matrix. Since the elements constituting the matrix are either $\{-1, 1\}$ or $\{-1, 0, 1\}$, only N^2 bits are needed to store the measurement matrix. Table 3 summarizes the complexity of these types of measurement matrices.

TABLE 3. Memory requirements and complexity.

Matrices	Variable	Storage
VCM	$2N$	$N + Nlog_2N$
GM	N^2	nN^2
MCBM	$2N^2$	N^2
SBM	N^2	N^2
COM	N^2	N^2
LTSBM	N^2	N^2
BM-C	N^2	N^2

The time complexity of the measurement matrix construction algorithm presented in this paper is analyzed based on its dimensionality, which is $N \times N$. Given that the sequence length necessary for matrix generation is only $2N$, the algorithm, despite involving multiple loops, does not contain nested loops. Consequently, the time complexity can be expressed as $O(2N) + O(N) + O(N-1) + O(N)$. The first term corresponds to the loop for generating the initial binary pseudo-random sequence. The second term represents the complexity of the XOR operation loop, the third term pertains to the Householder transformation, and the final term is associated with the random column inversion operation. It is evident that the dominant term in this complexity is $O(N)$. In contrast, matrices such as GM, COM, SBM, LTSBM, and BM-C require up to N^2 loops during their construction, and MCBM necessitates two rounds of N^2 loops. This results in a time complexity of $O(N^2)$ for these matrices, which is higher than the time complexity of our proposed algorithm. Regarding memory usage, the program's memory consumption primarily stems from storing the initial sequence for matrix construction, the binary Toeplitz matrix, the N-dimensional orthogonal matrix post-Householder transformation and sign function processing, the inverted coefficients, and the final measurement matrix. Thus, the memory requirement is $3N + 3N^2$ bytes.

VI. SIMULATION EXPERIMENTS AND PERFORMANCE EVALUATION

A. EVALUATION INDICATORS

This paper uses Compression Ratio (CR), Percent root means square difference (PRD), Signal-to-Noise Ratio (SNR) and Reconstruction rate as performance evaluation indicators. For the original signal with length N, and M observation points.

CR is the ratio of the length of the compressed signal to the length of the original signal. A higher CR makes reconstruction more challenging. The calculation formula is as follows:

$$CR = \frac{N - M}{N} \times 100\% \tag{43}$$

PRD measures the difference between the reconstructed signal x_r and the original signal x_o. The calculation formula is as follows:

$$PRD = \frac{\|x_o - x_r\|_2}{\|x_o\|_2} \times 100\% \tag{44}$$

SNR is crucial for assessing signal quality. It represents the ratio of the relative strength or power of the signal to noise. A higher SNR indicates better signal quality. SNR is calculated as follows:

$$SNR = 20\log\left(\frac{\|x_o\|_2}{\|x_o - x_r\|_2}\right) \tag{45}$$

Reconstruction rate signifies the probability of accurately restoring the target signal in multiple signal reconstruction experiments. The mathematical expression for Reconstruction rate is:

$$Rt = \frac{Success\ times}{Total\ times} \times 100\% \tag{46}$$

B. CHAOTIC MAPS TEST

To investigate the impact of chaotic map selection on matrix performance, this section's experiments utilize various chaotic mappings to construct the VCM, including the Logistic map, Chebyshev map, Bernoulli map, PWLCM map, Circle map, Iterative map, Cubic map, Fuch map, Singer map, Sine map, Tent map, Henon map, 2D-Logistic map, and Duffing map. A sparse test signal of length $N = 256$ and sparsity $K = 15$ is selected, where the positions of non-zero values are randomly determined and their magnitudes follow a normal distribution. During the statistical evaluation with observation points M ranging from 30 to 100, the performance variations of VCMs constructed using different chaotic maps are analyzed. The Orthogonal Matching Pursuit (OMP) algorithm [36] is chosen for signal recovery, and the experiment is repeated 1000 times. The success rate of reconstruction is statistically assessed. Fig. 2 illustrates that there is no significant difference in the performance of VCMs constructed using common chaotic maps. This outcome is attributed to the reliance on the chaotic sequence's superior properties during construction, rather than the specific values.

C. INITIAL CONDITION SENSITIVITY TEST

To investigate the impact of the initial state of the chaotic map on the measurement matrix's performance, 12 different combinations of initial values are randomly chosen for experimentation. The specific parameters selected are detailed in Table 4. Simultaneously, the observation point is set at $M = 120$ with a length of 256. Adjust the sparsity level K from a value of 10 to 80. A total of 1000 repeated experiments are conducted on the measurement matrices created under the 12 different initial value conditions. The *Reconstruction rates* of the various matrices under different sparsity are statistically analyzed. The outcomes are illustrated in Fig. 3. The figure demonstrates that variations in the initial value

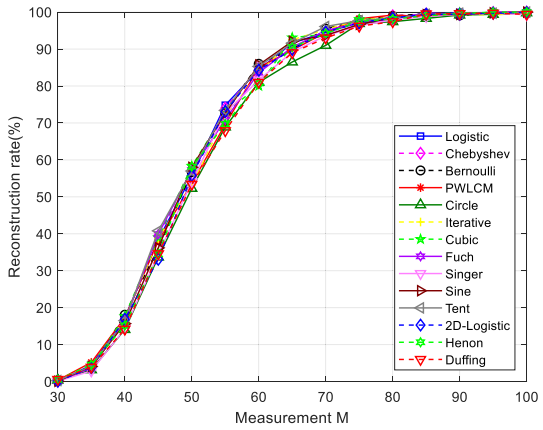

FIGURE 2. Performance of VCM based on different maps.

TABLE 4. Initial value selection for chaotic maps.

Group	Initial values	Group	Initial values
A	0.12	G	-0.57
B	-0.35	H	-0.6
C	-0.52	I	0.15
D	0.7	J	-0.2
E	0.3	K	0.68
F	0.8	L	-0.84

do not impact the reconstruction performance, with the measurement matrix performing consistently well across different initial values.

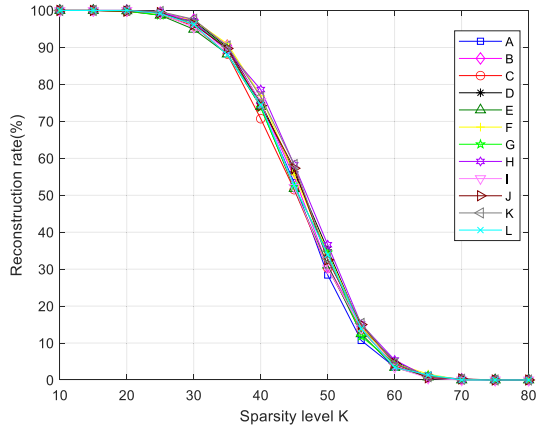

FIGURE 3. *Reconstruction rate* of chaotic map under different initial values, where $M = 120$, $N = 256$, and matrix = VCM.

D. SIGNAL RECOVERY EXPERIMENT

1) NOISE-FREE SIGNAL TESTING EXPERIMENT

In order to comprehensively evaluate the performance of the measurement matrix constructed in this paper, comparative experiments were conducted using the GM as the benchmark against the COM, SBM, LTSBM, MCBM and BM-C. In each experiment round, a random sequence of length $N = 256$ with sparsity $K = 20$ is generated. This implies that the signal contains 20 non-zero random values distributed according to a Gaussian distribution, with random positions. The signal exhibits sparsity under common transformations. The OMP algorithm is employed to recover the signal after compression sampling using the different measurement matrices where the sparsity level is set to M. A successful recovery is defined as when the positions of non-zero elements in the restored sparse vector x_r exactly match those in the original signal x_o, ensuring that the PRD is within the machine's acceptable precision range, that is, $PRD < 10^{-6}$, and simultaneously guaranteeing $SNR > 60dB$. If both requirements are met simultaneously, the recovery is deemed successful. Through 1000 iterations, this study records the probability of successfully reconstructing the signal using different measurement matrices. Subsequently, the reconstruction efficacy of each matrix is compared.

The simulation experiment is conducted to generate Fig. 4. As illustrated by the results graph, the reconstruction capability of the matrix constructed in this paper consistently outperforms that of other measurement matrices across varying measurement values. Specifically, MCBM, SBM and LTSBM exhibit similar and superior effects compared to the GM, and VCM also outperform the COM when the number of observation points is limited. The VCM demonstrates effective sampling and reconstruction due to its low mutual coherence, aligning with the stringent mutual coherence boundaries calculated for each matrix in the previous section. The low correlation of the VCM ensures high-quality signal reconstruction.

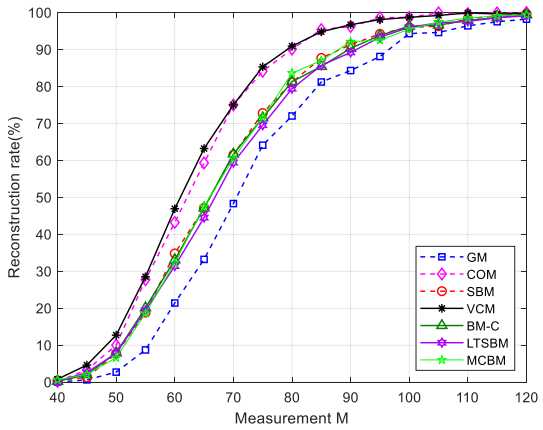

FIGURE 4. *Reconstruction rate* under different M, where $K = 20$, $N = 256$.

In order to thoroughly compare matrix performance, along with the aforementioned experiments, we chose a signal with a fixed length of $N = 256$ and $M = 40$ observation points. By varying the sparsity K from 2 to 22, we computed the reconstruction rate for different levels of sparsity. After conducting 1000 repeated experiments, the outcomes are illustrated in Fig. 5. With the same number of observation points and sparsity, VCM consistently exhibits a higher reconstruction rate. The six measurement matrices share a common trait: they all exhibit nearly perfect reconstruction rates when $K = 2$, but lose this ability completely when $K = 22$. However, in contrast to the previous experiment, SBM, BM-C, and MCBM perform slightly better than LTSBM. Due to their similar correlations, these three types of matrices still

demonstrate comparable performance. In this comparative experiment, the VCM continues to display exceptional performance. Under conditions of low sparsity, the performance of the VCM surpasses that of the COM. However, as the value of K escalates, the performance characteristics of both matrices converge, yet they consistently outperform other matrices.

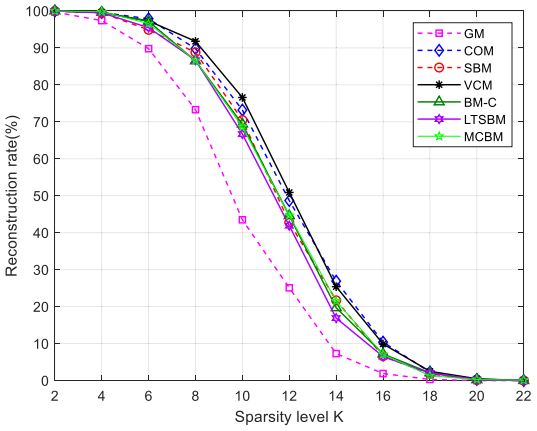

FIGURE 5. *Reconstruction rate* **under different sparsity level K, where $M = 40, N = 256$.**

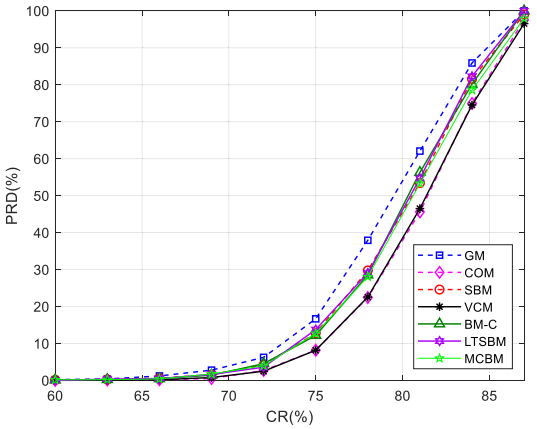

FIGURE 6. ***PRD*** **under different CR, where $K = 20, N = 256$.**

Simultaneously, the *PRD* for different measurement matrices at various *CRs* is calculated. Through 1000 iterations of experiments, the mean *PRD* is considered as the key metric, and the statistical results are presented in Fig. 6. The PRD serves as an indicator of the signal reconstruction accuracy. At lower *CRs*, all matrices exhibit the ability to compress and reconstruct the signal with minimal error and a high success rate. As the *CR* increases, the VCM and COM maintains a lower *PRD* compared to the other matrices. This observation highlights the favorable performance of the measurement matrix constructed in this paper even with a relatively low number of observations.

2) NOISE SIGNAL TESTING EXPERIMENT

In the simulation experiment of this section, we examine the model of a noisy signal $y = \Phi x + \omega$, where y represents the observed signal with Gaussian white noise, x is the original signal, and ω is Gaussian white noise. This experiment generates a test signal with a length of 256 and a sparsity of 10, a fixed observation value $M = 50$, and varies the SNR value from $10dB$ to $40dB$. The *PRD* under different *SNR* is recorded. The simulation results are depicted in Fig. 7. As the *SNR* increases, the *PRD* decreases, and the VCM developed in this paper consistently exhibits a lower *PRD*. When the *SNR* is low, the recovery performance of SRM surpasses that of SBM, BM-C, and LTSBM. With increasing *SNR*, the recovery performances of these matrices become more comparable. In conclusion, the VCM established demonstrates superior stability and recovery performance in the presence of external noise interference. COM can also achieve similar performance.

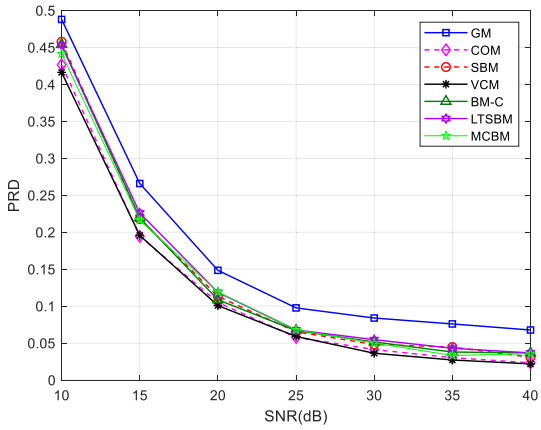

FIGURE 7. ***PRD*** **under different *SNR*, where $K = 10, N = 256, M = 50$.**

3) RECOVERY ALGORITHM TEST

There are various types of recovery algorithms for compressed sensing, and their effects vary. This study compares OMP, Basis Pursuit (BP) [37], Regularized Orthogonal Matching Pursuit (ROMP) [38], generalized Orthogonal Matching Pursuit (gOMP) [39], and Subspace Pursuit (SP) algorithms [40] through experiments. Keeping the number of observation points fixed at $M = 128$, the sparsity K is varied from 10 to 90. The results are depicted in Fig. 8, showing that gOMP yields the best results. gOMP, a generalization of OMP, differs in that it selects multiple maximum values at each step instead of just one with the largest correlation with the residual. This approach leads to a quicker reconstruction time by selecting multiple atomic times at fixed positions. By incorporating a regularization process based on OMP, gOMP significantly reduces complexity. Similarly, ROMP selects multiple column vectors most relevant to the residuals in each iteration. SP, an optimization algorithm of CoSaMP, demonstrates higher calculation efficiency. The figure illustrates that SP outperforms OMP but lags behind gOMP. Another significant category of CS reconstruction algorithms involves convex optimization or optimal approximation methods. These methods approximate

the signal by transforming non-convex problems into convex ones. Among these, the BP algorithm is the most commonly utilized. Despite its high complexity and long running time, it outperforms the OMP algorithm when dealing with a small number of observation points.

At the same time, the time taken for each recovery algorithm to conduct 100 rounds of experiments is calculated, and the outcomes are displayed in Fig. 9. The execution time of the BP algorithm significantly surpasses that of other recovery algorithms. The recovery duration of the OMP and gOMP algorithms steadily rises with the growth of sparsity, whereas the execution time of the ROMP algorithm remains relatively constant with minimal fluctuations.

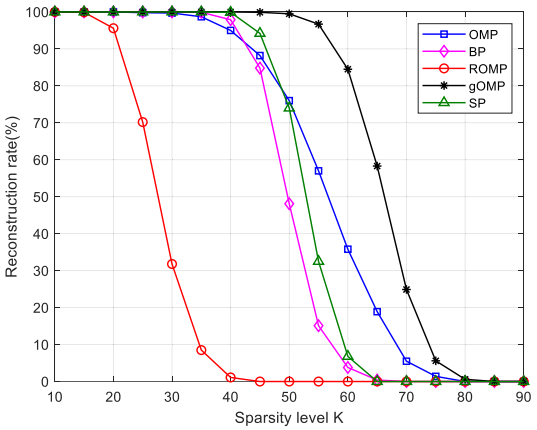

FIGURE 8. ***Reconstruction rate*** **of different reconstruction algorithms, where** $M = 128$, $N = 256$, **and matrix = VCM.**

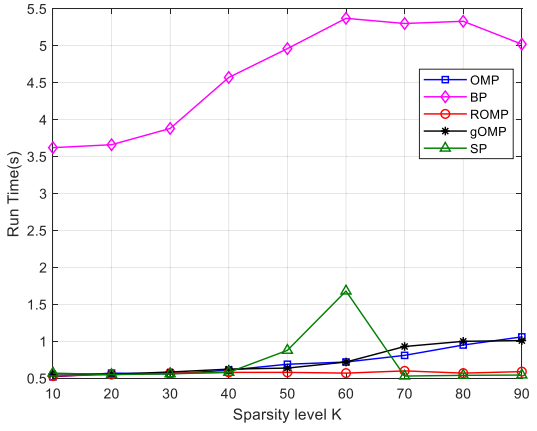

FIGURE 9. ***Run Time*** **of different reconstruction algorithms, where** $M = 128$, $N = 256$, **and matrix = VCM.**

To investigate the convergence properties of the measurement matrix developed in this study when reconstructed using various algorithms under both ideal and noisy conditions, experiments are conducted with a generation length of 256, sparsity level of 30, 80 observation points, and iteration counts ranging from 1 to 30. Each experiment is repeated 1000 times to calculate the *PRD* between the reconstructed and original signals for different iteration counts. The average *PRD* from 1000 trials is recorded. In an ideal noise-free environment, the discrepancy between the reconstructed signal and the original, using the matrix constructed herein across different algorithms and iteration counts, is assessed. Results, presented in Fig. 10, indicate that as the number of iterations increases, the error diminishes and stabilizes for Sparsity Adaptive Matching Pursuit (SAMP), OMP, SP, and gOMP. With the ROMP algorithm, the matrix fails to reconstruct the signal under these conditions, resulting in a *PRD* consistently at 1. The convergence of the measurement matrix, when generated by the proposed algorithm and utilized in the SAMP reconstruction algorithm, exhibits less sensitivity to variations in the number of iterations compared to other algorithms. There will be instances where similar effects arise at varying numbers of iterations. Overall, the algorithm exhibits commendable convergence when employing the gOMP algorithm for signal reconstruction.

In subsequent experiments, conditions are adjusted to incorporate noise, specifically at a *SNR* of 20dB, while other parameters remained constant. The outcomes of these experiments are depicted in Fig. 11. Similar to the noise-free scenario, the error decreases and stabilizes for both OMP and gOMP as iterations increase. However, the performance of the measurement matrix shifts from stable to unstable when using the SP algorithm. Likewise, the ROMP algorithm proves ineffective for reconstruction under these noisy conditions. The convergence behavior of the SAMP algorithm under noisy conditions varies significantly with the number of iterations, which is markedly different from the convergence under noise-free conditions. As the number of iterations increases, the performance of SAMP tends to outperform that of other algorithms.

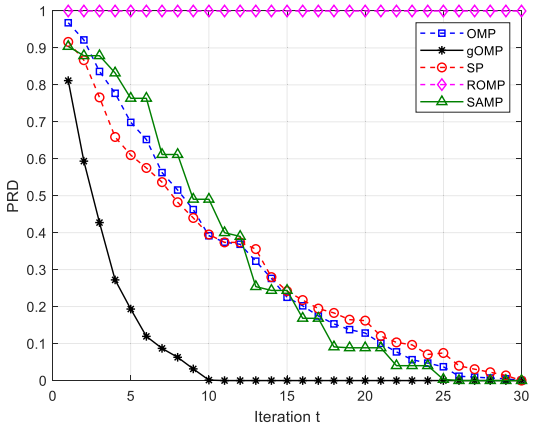

FIGURE 10. ***PRD*** **of different Iterations** t, **where** $M = 80$, $N = 256$, $K = 30$ **and matrix = VCM.**

4) RUN TIME TEST

In this study, a random signal of length $N = 256$ and $K = 20$ is generated, and the observation value M is varied from 40 to 100. The experiment is conducted 1000 times for each observation point, and the total time required is recorded as the outcome. GM is a non-deterministic matrix, necessitating the generation of random numbers for each

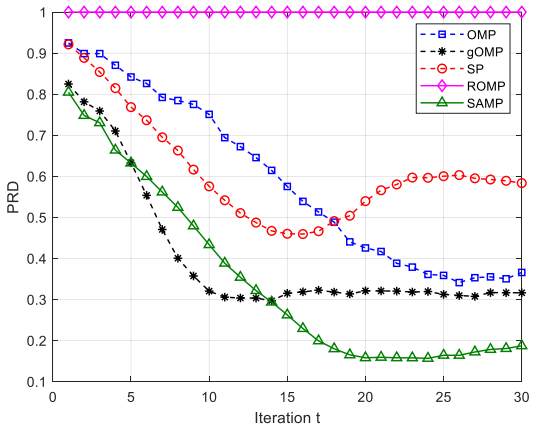

FIGURE 11. *PRD* of different Iterations t, where $M = 80$, $N = 256$, $K = 30$, $SNR = 20dB$ and matrix = VCM.

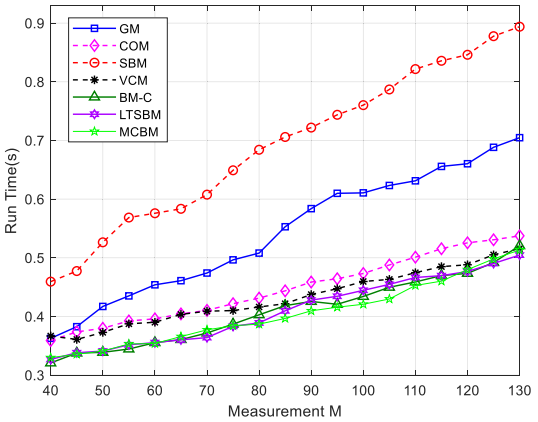

FIGURE 12. *Run Time* under different measurement M, where $K = 20$, $N = 256$.

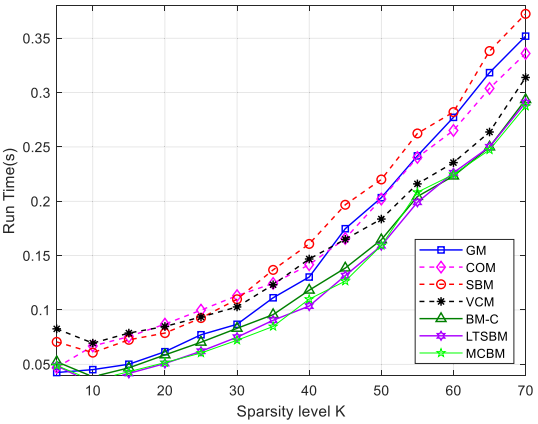

FIGURE 13. *Run Time* under different sparsity level K, where $M = 100$, $N = 256$.

iteration of the experiment. Consequently, as the number of experiments grows, the runtime also increases. Similarly, for SBM, it is essential to randomly select rows of the acquisition matrix in each experiment round to create the measurement matrix, leading to an increase in runtime. With an increase in the observation value, the number of matrix elements of BM-C and LTSBM rises, indicating that a longer chaotic sequence is needed to construct the matrix, resulting in a longer runtime. The complexity of generating BM-C is lower than that of LTSBM, leading to a shorter runtime. As VCM is a deterministic matrix, the initial value selection does not impact matrix performance in the experimental validation of the aforementioned sections. Once the initial value of the chaotic map is set, the matrix is fixed, requiring fewer initial variables. With high observation values, matrix construction and compression reconstruction can be accomplished more quickly. However, compared to other deterministic matrices, the speed difference in construction with VCM is at the millisecond level. The MCBM matrix offers the benefit of reducing power consumption while maintaining performance, effectively decreasing runtime. The simulation results are depicted in Fig. 12. Adjusting the matrix dimension significantly influences the computational complexity of the matrix construction algorithm, which in turn directly impacts the execution time. Consequently, the VCM approach enhances the matrix construction technique, preserving matrix performance while achieving increased efficiency.

Concurrently, a control experiment has been implemented to assess the impact of sparsity on reconstruction time. With the matrix dimension $M = 100$ held constant, the sparsity K of the test sequence is systematically varied, and the time expenditure for 100 iterations of the experiment is recorded. Fig. 13 illustrates the findings. At lower sparsity levels, the VCM exhibits a comparatively longer reconstruction time. However, as sparsity K escalates, the reconstruction velocity of VCM surpasses that of COM, GM, and SBM, and it remains closely competitive with BM-C, LTSBM, and MCBM, demonstrating a minimal performance gap. In conclusion, VCM effectively reconciles the trade-off between performance and efficiency.

5) IMAGE RECONSTRUCTION EXPERIMENT

Similar to the one-dimensional signal reconstruction experiment, this section primarily assesses the reconstruction performance of the measurement matrix constructed in this article for two-dimensional images. The non-sparse images Cameraman, Goldhill, and Peppers are chosen as representatives, all with sizes of 256 × 256. When conducting sparse representation, different function spaces such as Fourier transform, wavelet transform, or multi-scale geometric analysis are typically utilized to analyze the signal. The SL0 algorithm for CS reconstruction utilizes a smooth ℓ_0 norm and introduces a series of smooth functions to approximate the ℓ_0 norm [41]. Reference [42] introduces an optimization algorithm MSL0 based on the SL0 algorithm. This approach incorporates a hard threshold operator to prevent local minima and expedite convergence. The paper adopts MSL0 as the image restoration algorithm.

The Peak Signal-to-Noise Ratio (PSNR) of the two-dimensional image is employed to assess the quality of the reconstructed image [43]. The calculation formula is as

follows:

$$PSNR = 20log\frac{255}{(1/MN)\sum_{i=0}^{M-1}\sum_{j=0}^{N-1}[(x_o(i,j)-x_r(i,j))]^2} \tag{47}$$

In this experiment, we use Discrete Wavelet Transform (DWT) [44] to apply sparse processing to the image, aiming to more intuitively demonstrate the quality of each image after VCM compression and reconstruction at different *CRs*. Fig. 14 depicts the reconstruction effect. When $CR > 50\%$, the quality of the image restoration effect is higher.

Structural Similarity (SSIM) models distortion in images by considering brightness, contrast, and structure as key factors [45]. Brightness is estimated using the mean, contrast using the standard deviation, and structural similarity using the covariance. The values of SSIM are in the interval [0, 1], with higher values indicating less difference between images. Calculated as follows:

$$SSIM = \frac{(2\mu_{x_o}\mu_{x_r}+c_1)(2\sigma_{x_ox_r}+c_2)}{\left(\mu_{x_o}^2+\mu_{x_r}^2+c_1\right)\left(\sigma_{x_o}^2+\sigma_{x_r}^2+c_2\right)} \tag{48}$$

The calculation involves μ_{x_o} and μ_{x_r} as the mean values of x_o and x_r, σ_{x_o}, σ_{x_r} and $\sigma_{x_ox_r}$ as the variances of x_o and x_r along with their covariance, and constants c_1, c_2 for stability. In this study, we counted the *SSIM* values of the restored image and the original image under different *CRs*, and the DCT matrix is used as a sparse matrix, with the MSL0 restoration algorithm. By adjusting the *CR* value, *SSIM* values under different conditions were recorded. The statistical findings are presented in Table 5. Goldhill exhibited the best sparsity characteristics after the sparse process, followed by Peppers, while Cameraman still showed poor sparsity. For images with better sparsity like Peppers and Goldhill, all six matrices showed improved reconstruction quality, yet the VCM consistently yielded the best *SSIM* values. In the case of the Cameraman image with poor sparsity, the VCM demonstrated significantly enhanced processing performance compared to other matrices. As *CR* increases, the number of observation points gradually decreases, and the *SSIM* value also decreases. This trend is due to the fact that fewer sampling points lose more information about the image, resulting in poor recovery. When *CR* is low, the measurement matrices effectively restore the images. As the *CR* increases, the VCM effect outperforms other measurement matrices.

At the same time, the recovery algorithm is switched to the OMP algorithm, and the experiment is repeated. The results are displayed in Table 6. It is evident that under identical conditions, the recovery performance of the MSL0 algorithm surpasses that of the OMP algorithm, aligning with the findings of the prior study. Nevertheless, the OMP algorithm exhibits a shorter runtime compared to the MSL0 algorithm. Similar to the restoration using the MLS0 algorithm, as the *CR* increases, the restoration effect of each measurement matrix worsens, especially when processing images with lower sparsity like Cameraman.

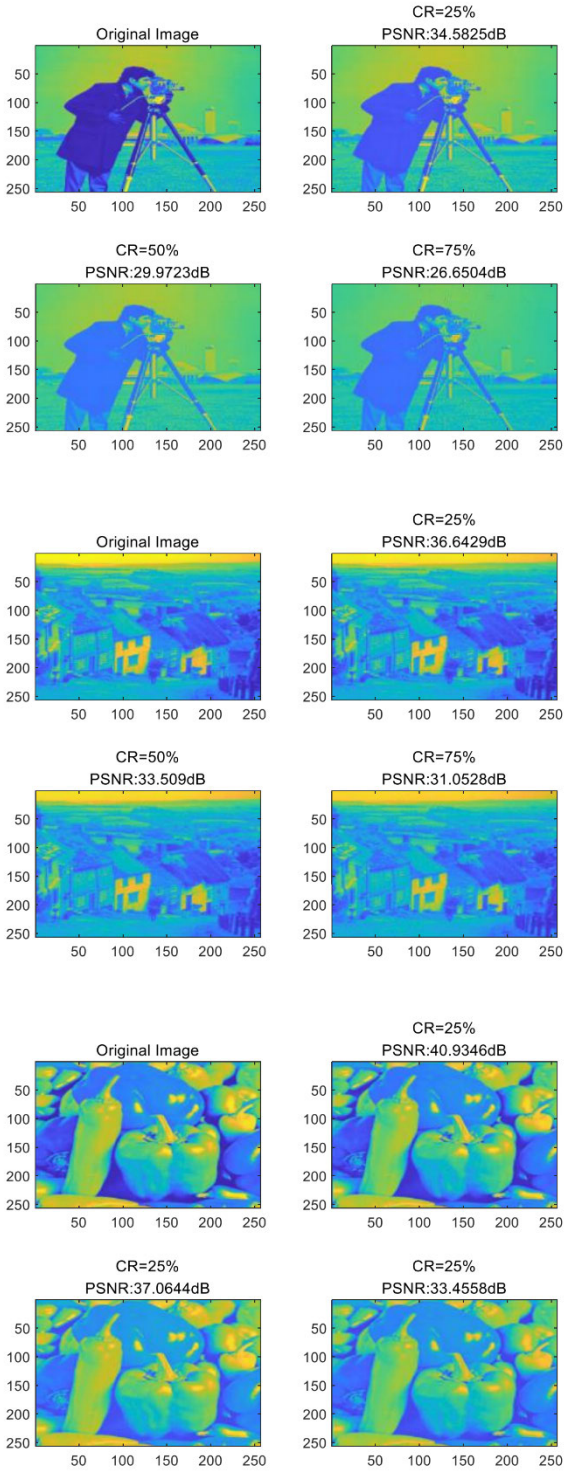

FIGURE 14. Cameraman, Goldhill and Peppers images reconstructed through VCM.

When employing the OMP algorithm for image restoration, the VCM presented in this study demonstrates a significantly superior effect compared to GM, SBM, BM-C, MCBM, and LTSBM, and slightly outperforms COM. However, this advantage is less pronounced when utilizing the MLS0 algorithm for restoration.

TABLE 5. SSIM values for different measurement matrices based on MLS0.

Images	Matrices	CR=25%	CR=50%	CR=75%
Cameraman	GM	0.4419	0.2979	0.1509
	COM	0.4396	0.2997	0.1552
	SBM	0.4401	0.3005	0.1553
	VCM	**0.4455**	**0.3052**	**0.1608**
	BM-C	0.4432	0.2993	0.1580
	LTSBM	0.4424	0.2998	0.1518
	MCBM	0.4409	0.2989	0.1576
Goldhill	GM	0.7176	0.4999	0.2707
	COM	0.7169	0.5074	0.2756
	SBM	0.7198	0.5084	0.2702
	VCM	**0.7211**	**0.5109**	**0.2711**
	BM-C	0.7158	0.5075	0.2620
	LTSBM	0.7199	0.4970	0.2731
	MCBM	0.7244	0.5000	0.2701
Peppers	GM	0.6487	0.4660	0.2175
	COM	0.6546	0.4623	0.2252
	SBM	0.6547	0.4672	0.2224
	VCM	**0.6590**	**0.4704**	**0.2334**
	BM-C	0.6585	0.4693	0.2298
	LTSBM	0.6556	0.4685	0.2299
	MCBM	0.6583	0.4679	0.2263

TABLE 6. SSIM values for different measurement matrices based on OMP.

Images	Matrices	CR=25%	CR=50%	CR=75%
Cameraman	GM	0.3202	0.2290	0.1101
	COM	0.3533	0.2331	0.1141
	SBM	0.3244	0.2282	0.1138
	VCM	**0.3572**	**0.2430**	**0.1168**
	BM-C	0.3247	0.2253	0.1140
	LTSBM	0.3258	0.2228	0.1113
	MCBM	0.3208	0.2252	0.1118
Goldhill	GM	0.5443	0.3928	0.1773
	COM	0.5889	0.4102	0.2084
	SBM	0.5410	0.3721	0.2042
	VCM	**0.5960**	**0.4209**	**0.2051**
	BM-C	0.5408	0.3810	0.2013
	LTSBM	0.5444	0.3851	0.1899
	MCBM	0.5377	0.3955	0.1888
Peppers	GM	0.5065	0.3560	0.1589
	COM	0.5596	0.3991	0.1630
	SBM	0.5106	0.3672	0.1716
	VCM	**0.5602**	**0.3970**	**0.1745**
	BM-C	0.5025	0.3704	0.1651
	LTSBM	0.5059	0.3613	0.1581
	MCBM	0.5080	0.3693	0.1574

VII. CONCLUSION

This paper addresses key challenges associated with traditional matrices in compressed sensing, including suboptimal compression performance under non-ideal sparsity conditions, the complexities inherent in the hardware implementation of random measurement matrices, and the substantial storage space requirements. To this end, we introduce a novel method for constructing a deterministic measurement matrix predicated on chaotic sequences. Specifically, a nonlinear binary sequence transformation method is used, and the Householder transformation is employed in matrix construction, yielding a matrix that fulfills the Restricted Isometry Property (RIP). The proposed method offers numerous benefits: (1) It leverages chaotic sequences with high complexity and robust randomness, thereby mitigating storage inefficiencies associated with sampling intervals in conventional matrices. (2) It surmounts the stringent system requirements for random number generation and the storage and transmission of measurement matrices during the compression and reconstruction phases. (3) The proposed deterministic matrix exhibits a higher likelihood of satisfying the RIP criteria compared to matrices such as Gaussian random matrices. Empirical results substantiate that the matrix can achieve a higher success rate in signal reconstruction, even under conditions of low sparsity or limited observation points, coupled with reduced processing time and enhanced reconstruction quality. (4) The matrix excels not only in signal reconstruction but also in image compression and reconstruction, significantly improving the PSNR and SSIM metrics of reconstructed images, particularly in scenarios characterized by poor sparsity. (5) The performance of the matrix is invariant to the initial value, rendering it apt for cryptographic key generation. Additionally, its application in various signal processing domains is promising, and further research into the hardware implementation of these pseudo-random chaotic matrices is warranted.

REFERENCES

[1] D. L. Donoho, "Compressed sensing," *IEEE Trans. Inf. Theory*, vol. 52, no. 4, pp. 1289–1306, Apr. 2006.
[2] V. S. Unni, R. G. Gavaskar, and K. N. Chaudhury, "Compressive sensing of ECG signals using plug-and-play regularization," *Signal Process.*, vol. 202, Jan. 2023, Art. no. 108738.
[3] Z. Zha, B. Wen, X. Yuan, J. Zhang, J. Zhou, and C. Zhu, "Structured residual sparsity for video compressive sensing reconstruction," *Signal Process.*, vol. 222, Sep. 2024, Art. no. 109513.
[4] M.-S. Kang and J.-M. Baek, "SAR image reconstruction via incremental imaging with compressive sensing," *IEEE Trans. Aerosp. Electron. Syst.*, vol. 59, no. 4, pp. 4450–4463, Aug. 2023.
[5] E. J. Candes and T. Tao, "Decoding by linear programming," *IEEE Trans. Inf. Theory*, vol. 51, no. 12, pp. 4203–4215, Dec. 2005.
[6] E. J. Candes, J. Romberg, and T. Tao, "Robust uncertainty principles: Exact signal reconstruction from highly incomplete frequency information," *IEEE Trans. Inf. Theory*, vol. 52, no. 2, pp. 489–509, Feb. 2006.
[7] W. Lu, W. Li, K. Kpalma, and J. Ronsin, "Compressed sensing performance of random Bernoulli matrices with high compression ratio," *IEEE Signal Process. Lett.*, vol. 22, no. 8, pp. 1074–1078, Aug. 2015.
[8] G. Xu and Z. Xu, "Compressed sensing matrices from Fourier matrices," *IEEE Trans. Inf. Theory*, vol. 61, no. 1, pp. 469–478, Jan. 2015.
[9] G. Wang, M.-Y. Niu, and F.-W. Fu, "Deterministic constructions of compressed sensing matrices based on optimal codebooks and codes," *Appl. Math. Comput.*, vol. 343, pp. 128–136, Feb. 2019.
[10] H. Abin, F. Shahrivari, and A. Amini, "Explicit matrices with low coherence based on algebraic geometric codes," *Signal Process.*, vol. 212, Nov. 2023, Art. no. 109173.
[11] S. Zhu, C. Zhu, H. Cui, and W. Wang, "A class of quadratic polynomial chaotic maps and its application in cryptography," *IEEE Access*, vol. 7, pp. 34141–34152, 2019.
[12] J. Jin, L. Xing, J. Shen, R. Li, M. Yang, and Z. Zhou, "Design of a dynamic sparse circulant measurement matrix based on a new compound sine chaotic map," *IEEE Access*, vol. 10, pp. 10827–10837, 2022.
[13] H. Gan, Z. Li, J. Li, X. Wang, and Z. Cheng, "Compressive sensing using chaotic sequence based on Chebyshev map," *Nonlinear Dyn.*, vol. 78, no. 4, pp. 2429–2438, Dec. 2014.
[14] S. Patel and A. Vaish, "Block based visually secure image encryption algorithm using 2D-compressive sensing and nonlinearity," *Optik*, vol. 272, Feb. 2023, Art. no. 170341.
[15] Y. Yan, K. Chen, Y. Zhao, H. Wang, B. Xu, and Y. Wang, "An innovative orthogonal matrix based on nonlinear chaotic system for compressive sensing," *Chaos, Solitons Fractals*, vol. 178, Jan. 2024, Art. no. 114319.

[16] K. Chatterjee, H. Fu, A. K. Goharshady, and E. K. Goharshady, "Polynomial invariant generation for non-deterministic recursive programs," in *Proc. 41st ACM SIGPLAN Conf. Program. Lang. Design Implement.*, vol. 14, Jun. 2020, pp. 672–687.
[17] E. J. Candès, "The restricted isometry property and its implications for compressed sensing," *Comptes Rendus Math.*, vol. 346, nos. 9–10, pp. 589–592, Apr. 2008.
[18] J. M. Duarte-Carvajalino and G. Sapiro, "Learning to sense sparse signals: Simultaneous sensing matrix and sparsifying dictionary optimization," *IEEE Trans. Image Process.*, vol. 18, no. 7, pp. 1395–1408, Jul. 2009.
[19] S. Ghosh, P. Pal, and N. Kar, "An analysis of chaos-based cryptographic algorithms," in *Proc. 5th Int. Conf. Elect., Comput. Commun. Technol. (ICECCT)*, 2023, pp. 1–7.
[20] J. Haupt, W. U. Bajwa, G. Raz, and R. Nowak, "Toeplitz compressed sensing matrices with applications to sparse channel estimation," *IEEE Trans. Inf. Theory*, vol. 56, no. 11, pp. 5862–5875, Nov. 2010.
[21] T. T. Do, L. Gan, N. H. Nguyen, and T. D. Tran, "Fast and efficient compressive sensing using structurally random matrices," *IEEE Trans. Signal Process.*, vol. 60, no. 1, pp. 139–154, Jan. 2012.
[22] G. E. P. Box and M. E. M$^{\prime}$uller, "A note on the generation of random normal deviates," *Ann. Math. Statist.*, vol. 29, no. 2, pp. 610–611, Jun. 1958.
[23] T. Kohda, "Stream cipher systems using a chaotic sequence of IID random variables (5th workshop on stochastic numerics)," *Proc. Inst. Math. Sci.*, vol. 1240, pp. 74–87, Dec. 2001.
[24] N. H. Augustin, E.-A. Sauleau, and S. N. Wood, "On quantile quantile plots for generalized linear models," *Comput. Statist. Data Anal.*, vol. 56, no. 8, pp. 2404–2409, Aug. 2012.
[25] A. A. Dubrulle, "Householder transformations revisited," *SIAM J. Matrix Anal. Appl.*, vol. 22, no. 1, pp. 33–40, Jan. 2000.
[26] A. Rukhin, J. Soto, J. Nechvatal, M. Smid, E. Barker, S. Leigh, M. Levenson, M. Vangel, D. Banks, A. Heckert, J. Dray, and S. Vo, *A Statistical Test Suite for Random and Pseu-Dorandom Number Generators for Cryptographic Applications*. Gaithersburg, MD, USA: U.S. Department of Commerce, National Institute of Standards and Technology, 2001.
[27] C. Zhuoran, Z. Honglin, J. Min, W. Gang, and S. Jingshi, "An improved Hadamard measurement matrix based on Walsh code for compressive sensing," in *Proc. 9th Int. Conf. Inf., Commun. Signal Process.*, Dec. 2013, pp. 1–4.
[28] H. Pham, *Springer Handbook of Engineering Statistics*. London, U.K.: Springer, 2023.
[29] R. Baraniuk, M. Davenport, R. DeVore, and M. Wakin, "A simple proof of the restricted isometry property for random matrices," *Constructive Approximation*, vol. 28, no. 3, pp. 253–263, Dec. 2008.
[30] C. Yang, P. Pan, and Q. Ding, "Image encryption scheme based on mixed chaotic Bernoulli measurement matrix block compressive sensing," *Entropy*, vol. 24, no. 2, p. 273, Feb. 2022.
[31] H. Gan, S. Xiao, T. Zhang, and F. Liu, "Bipolar measurement matrix using chaotic sequence," *Commun. Nonlinear Sci. Numer. Simul.*, vol. 72, pp. 139–151, Jun. 2019.
[32] J. Zhang, L. Qiao, and Y. Wang, "Band measurement matrix based analog to information conversion," in *Proc. IEEE Int. Instrum. Meas. Technol. Conf. (I2MTC)*, May 2021, pp. 1–5.
[33] X. Jianhong, W. Cong, W. Linyu, and Z. Yu, "FECG compressed sensing mode based on joint block sparsity," *Biomed. Signal Process. Control*, vol. 86, Sep. 2023, Art. no. 105137.
[34] W. Hoeffding, "Probability inequalities for sums of bounded random variables," in *The Collected Works Wassily Hoeffding*. New York, NY, USA: Springer, 1994, pp. 409–426.
[35] A. Eftekhari, H. L. Yap, C. J. Rozell, and M. B. Wakin, "The restricted isometry property for random block diagonal matrices," *Appl. Comput. Harmon. Anal.*, vol. 38, no. 1, pp. 1–31, Jan. 2015.
[36] J. A. Tropp and A. C. Gilbert, "Signal recovery from random measurements via orthogonal matching pursuit," *IEEE Trans. Inf. theory*, vol. 53, no. 12, pp. 4655–4666, Dec. 2007.
[37] S. Chen and D. Donoho, "Basis pursuit," in *Proc. 28th Asilomar Conf. Signals, Syst. Comput.*, vol. 1, 1994, pp. 41–44.
[38] D. Needell and R. Vershynin, "Uniform uncertainty principle and signal recovery via regularized orthogonal matching pursuit," *Found. Comput. Math.*, vol. 9, no. 3, pp. 317–334, Jun. 2009.
[39] J. Wang, S. Kwon, and B. Shim, "Generalized orthogonal matching pursuit," *IEEE Trans. Signal Process.*, vol. 60, no. 12, pp. 6202–6216, Dec. 2012.
[40] W. Dai and O. Milenkovic, "Subspace pursuit for compressive sensing signal reconstruction," *IEEE Trans. Inf. Theory*, vol. 55, no. 5, pp. 2230–2249, May 2009.
[41] L. Wang, P. Ye, and J. Xiang, "A modified algorithm based on smoothed ℓ_0 norm in compressive sensing signal reconstruction," in *Proc. 25th IEEE Int. Conf. Image Process. (ICIP)*, Oct. 2018, pp. 1812–1816.
[42] S. Yang, Y. Zhao, X. Tuo, D. Mao, Y. Zhang, and J. Yang, "Real aperture radar angular super-resolution imaging using modified smoothed ℓ_0 norm with a regularization strategy," *Remote Sens.*, vol. 16, no. 1, p. 12, Dec. 2023.
[43] A. Horé and D. Ziou, "Image quality metrics: PSNR vs. SSIM," in *Proc. 20th Int. Conf. Pattern Recognit.*, Aug. 2010, pp. 2366–2369.
[44] N. Kashyap and G. R. Sinha, "Image watermarking using 3-level discrete wavelet transform (DWT)," *Int. J. Modern Educ. Comput. Sci.*, vol. 4, no. 3, pp. 50–56, Apr. 2012.
[45] C. Li and A. C. Bovik, "Three-component weighted structural similarity index," *Pro. SPIE*, vol. 7242, pp. 252–260, Jan. 2009.

XUANWEI ZHANG received the B.S. degree in communication engineering from Hunan Normal University, Changsha, China, in 2022, where he is currently pursuing the M.S. degree in communication engineering. His research interests include compressed sensing techniques and ultra-wideband (UWB) radar signal processing.

HUIMIN YU received the B.S. degree from Hunan Normal University, China, in 2003, the M.S. degree in engineering from Hunan University, in 2006, and the Ph.D. degree in electromagnetic fields and microwave technology from the Institute of Electronics, Chinese Academy of Sciences, in 2009. As a distinguished scholar, he worked as a Visiting Scholar at The University of Arizona, USA. Since 2018, he has been a teaching career at Hunan Normal University, where he is currently working as an Associate Professor with the College of Information Science and Engineering. His research interests include design of ultra-wideband systems and wireless communication networks.